Supplement of

Enigmatic Fe-Mn fueled Anaerobic Oxidation of Methane in sulfidic coastal sediments of the Eastern Arabian Sea

Kalyani Sivan[1,2], Aditya Peketi[1,2], Aninda Mazumdar[1,2]*, Anjali Zatale[1,2], Sai Pavan Kumar Pillutla [2,3], Ankita Ghosh[1,2], Mohd Sadique[2,3], Jittu Mathai[2]

[1]*Academy of Scientific and Innovative Research (AcSIR), Ghaziabad-201002, India*

[2]*Gas hydrate Research Group, CSIR-National Institute of Oceanography, Dona Paula, Goa-403004, India*

[3]*School of Earth, Ocean, and Atmospheric Sciences, Goa University, Taleigao Plateau, Goa- 403206, India*

Correspondence to: Dr. Aninda Mazumdar (maninda@nio.org)

This PDF file includes:

- Supporting text
- Figures S1 & S2
- Tables S1 to S3
- References

Supporting Information Text

Geological setting and Hydrography

The western continental margin of India is a passive NNW-SSE margin with a shelf break at 140-180m depth. The Western Continental Shelf of India (WCSI) covers an area of 0.3×10^6 km^2 and gently slopes to the west with a gradient of 1:400 to 1:3000 to a water depth of 140 m (Wagle et al., 1994). The inner shelf has a smooth and gently sloping topography with a gradient of 1:700 to 1:3300 and is characterized by organic carbon-rich silt and clay up to a water depth of 50 m. The mid shelf shows uneven topography and predominantly composed of calcareous oolitic sand (Nair et al., 1978). The outer shelf is composed of relict carbonate sediments, phosphatic limestone micronodules (Rao and Nair, 1988), low organic matter coarse sands, and high carbonates (Rao and Wagle, 1977). The width of the continental shelf varies significantly, spanning from 345 km off Daman to 100 km in northern Kutch, tapering to 120 km off Goa, and 60 km off Quilon in Kerala (Rao and Wagle, 1977). Previous studies (Siddiquie et al., 1981, Karisiddaiah et al., 2002) have identified gas-charged sediments along the WCSI. The sediments in the continental shelf of off Goa are characterized by high iron content due to large input of Fe oxyhydroxides in the shelf via Mandovi and Zuari estuaries, as a result of iron ore mining and processing along the West coast of India (Sebastian et al., 2017). The sedimentation rates reported from WCSI (off Goa) within a water depth of 40 m vary from 0.15 to 1.57 cm/yr (Nigam et al., 1995; Kurian et al., 2009; Mazumdar et al., 2012; Sebastian et al., 2017; Fernandes et al., 2020).

The WCSI experiences suboxia and denitrification over the inner and mid-shelf during and immediately after the southwest monsoon due to the strong upwelling of cold, nutrient-rich oxygen-deficient water from the south (Naqvi et al., 2000). The high primary productivity due to enhanced nutrient availability and subsequent respiration of excess organic matter leads to oxygen drawdown, resulting in hypoxia formation. This in conjunction with shallow thermohaline stratification, developed due to high rainfall (3000 mm) in the coastal zone and adjoining areas of Western Ghats further intensifies bottom water hypoxia. This seasonal hypoxic zone covers an area of 0.18 million sq. km and is the largest among all coastal hypoxic systems (Naqvi et al., 2000; Naqvi et al., 2006).

Supporting Figures

S1: Dissolved sulfide and iron in porewaters

Figure S1 shows the cross plot of dissolved iron (Fe) vs sulfide in porewaters reported from Fe-Mn-AOM zones in marine sediments and the present study. Previous studies have indicated that Fe^{2+} enrichment during Fe-AOM is typically confined to the methanogenic zone or below the sulfidization front, where Fe^{2+} accumulation in porewater is favored due to the absence of sulfide. The precipitation of iron monosulfide and pyrite from dissolved sulfide and iron suppresses and masks signatures of Fe (III)-driven AOM (Riedinger et al., 2014; Egger et al., 2015a; Egger et al., 2015b; Egger et al., 2016a; Egger et al., 2016b; Egger et al., 2017; Aromokeye et al., 2019; Luo et al., 2020). However, in the present study, high porewater sulfide concentrations (3.3 to 10.38 mM) are observed throughout the core, despite high dissolved Fe^{2+} concentrations. A similar observation was also reported by a previous study (Li et al., 2019). The accumulation of ferrous iron in the presence of high sulfide concentrations in the porewater possibly indicates a greater rate of Fe^{2+}-Mn^{2+} generation compared to their consumption via sulfidization (FeS/FeS_2; Hensen et al., 2003).

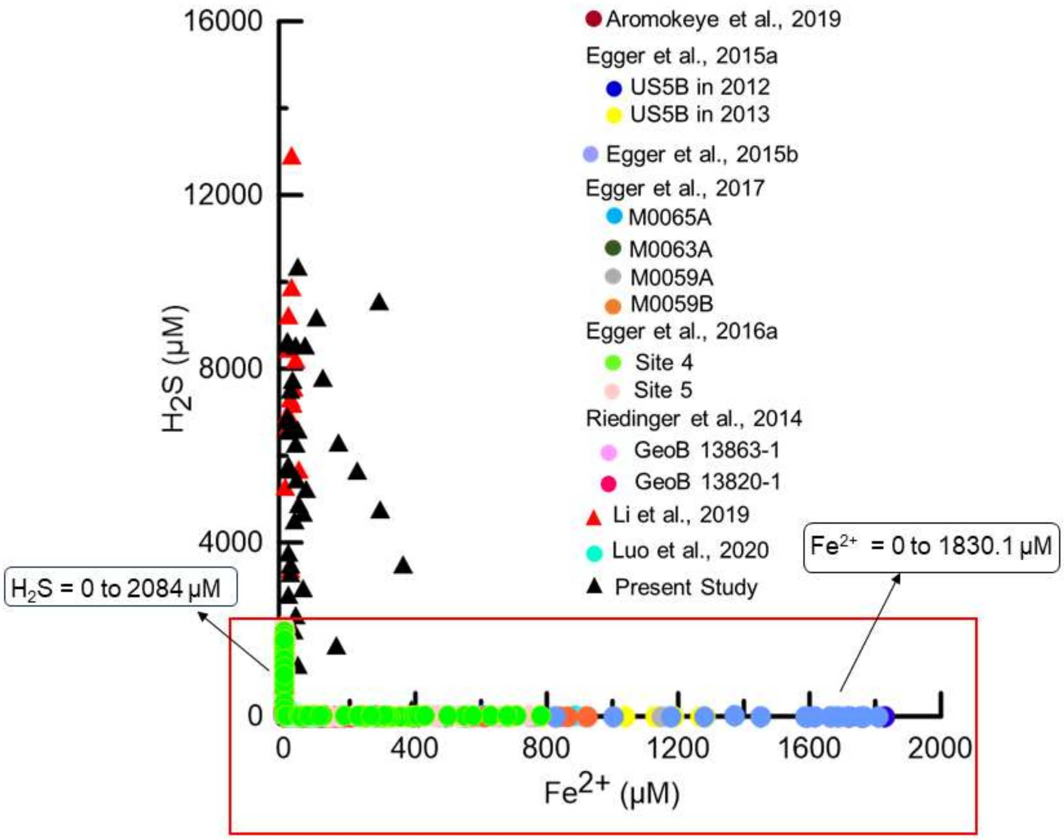

Figure S1. Cross plot of porewater Fe^{2+} and HS^- concentrations reported from Fe-Mn-AOM zones in marine sediments (Riedinger et al., 2014; Egger et al., 2015a; Egger et al., 2015b; Egger et al., 2016a; Egger et al., 2017; Aromokeye et al., 2019; Luo et al., 2020) and present study. The red rectangle represents very low H_2S and Fe^{2+} values.

S2: Sedimentary TOC, TOC/TN, $\delta^{13}C_{TOC}$, and $\delta^{15}N_{TN}$ values

Figure S2 shows downcore records of TOC, TOC/TN, $\delta^{13}C_{TOC}$, and $\delta^{15}N_{TN}$. The clay-silt-rich sediment core (SSD070/7/GC6) exhibits a gradual decline in TOC content (from 26 mg/g to 1.45 mg/g) with depth below the seafloor (Table S2). The TOC/TN molar ratios range from 3.5 to 27.3 (avg.: 14.5 ± 3.5). Interestingly, the $\delta^{13}C_{TOC}$ and $\delta^{15}N_{TN}$ profiles show significant variation throughout the core with values ranging from -20.693 to -25.934 ‰ and -3.3 to 7.7 ‰ respectively. The downcore marked variation in TOC, TOC/TN, $\delta^{13}C_{TOC}$, and $\delta^{15}N_{TN}$

indicates significant variation in terrestrial and marine organic matter input, denitrification and nitrogen fixation in the study area. Moreover, the $\delta^{13}C_{TOC}$ profile in the present and previous studies (Mazumdar et al., 2012; Fernandes et al., 2020) also shows an overall depletion trend with depth indicating more organic matter contribution from terrestrial influx. These variations reflect the complex and dynamic nature of biogeochemical processes and organic matter sources in the coastal waters of the WCSI.

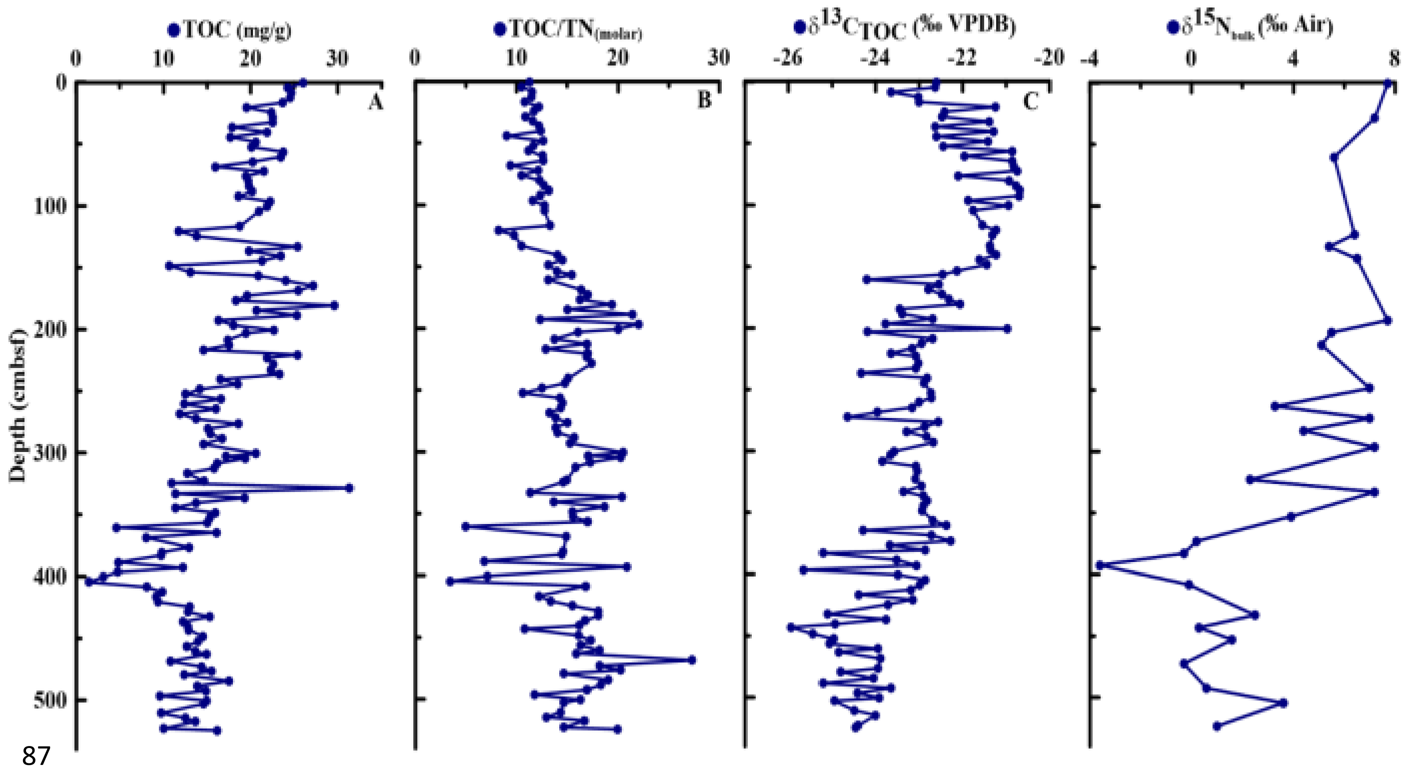

Figure S2. Vertical profiles of sedimentary a) TOC (in mg/g), b) $TOC/TN_{(molar)}$, c) $\delta^{13}C_{TOC}$ (‰ VPDB), and d) $\delta^{15}N$ (‰ Air) in the studied sediment core (SSD070/7/GC6).

Table S1. Porewater concentrations and carbon isotope ratio of methane ($\delta^{13}C_{CH4}$) and DIC ($\delta^{13}C_{DIC}$) in the studied core (SSD070/7/GC6). bdl= below detection limit, na= not analyzed.

Depth (cmbsf)	SO_4^{2-} (mM)	H_2S (µM)	CH_4 (µM)	$\delta^{13}C_{CH4}$ (‰ VPDB)	DIC (mM)	$\delta^{13}C_{DIC}$ (‰VPDB)	Fe (µM)	Mn (µM)
1	26.42	0.00	bdl	bdl	3.52	-9.60	129.59	24.90
8	25.29	0.00	bdl	bdl	4.81	-11.28	na	na
16	na	na	bdl	bdl	5.80	-13.23	48.56	17.37
23	23.30	0.00	bdl	bdl	5.97	-14.17	44.73	17.92
33	22.80	0.00	bdl	bdl	na	na	33.84	18.26
43	21.67	0.00	bdl	bdl	8.46	-9.78	9.05	9.08
53	19.59	0.00	bdl	bdl	8.11	-20.69	19.26	4.40
63	18.18	3300.97	bdl	bdl	8.08	-22.87	14.15	1.29
73	16.45	3756.29	bdl	bdl	8.16	-24.90	67.52	4.48
93	12.83	6595.17	bdl	bdl	8.76	-27.13	41.51	1.08
103	11.88	5451.93	bdl	bdl	8.34	-27.84	40.17	1.62
113	10.87	7791.28	bdl	bdl	8.48	-30.40	116.47	5.10
123	9.52	9186.08	bdl	bdl	9.30	-32.22	98.16	3.17
133	8.45	6310.23	165.44	-84.73	9.36	-33.77	164.95	4.83
143	7.77	8528.29	68.28	-87.14	10.58	-35.21	62.99	1.61
153	6.31	6576.81	bdl	bdl	9.80	-35.20	13.21	0.39
163	5.31	8529.26	bdl	bdl	10.46	-36.11	35.44	0.84
173	5.05	7525.84	151.34	-89.54	10.44	-36.01	18.67	0.44
183	4.39	8594.26	364.15	-86.35	na	na	13.09	0.33
193	3.97	6812.02	189.50	-91.88	10.69	-34.70	17.29	0.41

203	3.46	9563.97	bdl	bdl	12.77	-37.66	288.06	7.39
213	3.12	8782.92	111.53	-98.51	10.63	-34.86	na	na
223	2.94	6275.49	bdl	bdl	10.92	-36.14	34.97	0.78
233	2.40	8631.14	149.96	-101.92	11.14	-37.20	10.75	0.28
243	2.31	6901.46	bdl	bdl	11.44	-36.21	11.42	0.46
253	1.40	5672.54	120.87	-102.55	11.79	-36.70	11.27	0.39
263	1.06	7749.95	188.85	-105.55	11.31	-36.43	25.92	0.61
273	1.03	3483.98	175.47	-104.33	12.81	-37.99	361.28	5.51
283	0.56	6429.07	263.20	-103.76	11.37	-36.69	na	na
293	0.51	5852.16	369.86	-103.72	na	na	na	na
303	0.00046	5781.95	503.22	-98.60	10.53	-35.18	14.83	0.41
313	0.00040	bdl	647.41	-94.63	9.73	-32.17	na	na
323	0.00097	9249.26	3376.94	-86.15	na	na	na	na
333	0.00145	4768.08	673.33	-103.94	11.64	-34.14	293.25	2.47
343	0.00057	4875.69	895.83	-96.68	9.75	-31.37	43.90	2.43
353	0.00067	10345.89	1218.21	-91.43	9.70	-28.38	42.33	1.56
363	0.00076	3485.46	1521.38	-93.22	9.55	-26.51	20.89	0.96
373	0.00071	10385.61	1436.60	-87.76	9.85	-26.74	na	na
383	0.00075	5659.99	303.65	-109.59	11.08	-30.04	223.32	2.76
393	0.00051	1622.13	362.27	-110.96	9.46	-25.13	158.51	3.19
403	0.00049	2316.40	367.11	-109.59	8.34	-26.60	36.23	0.93
413	0.00041	2951.17	282.16	-110.82	8.07	-25.96	57.39	1.78
423	0.00055	bdl	891.00	-89.81	7.66	-22.46	124.16	4.31
433	0.00066	1432.59	1781.18	-69.66	7.10	-21.76	na	na
443	0.00059	163.78	372.89	-113.66	9.01	-23.96	387.55	10.17

453	0.00047	3757.41	2169.97	-69.20	6.98	-21.71	na	na
463	0.00079	4698.17	2276.94	-52.20	7.12	-21.29	58.22	2.68
473	0.00000	1984.93	403.82	-106.40	7.93	-23.61	29.90	1.65
483	0.00050	4520.32	206.61	-55.69	6.95	-21.72	33.22	1.55
493	0.00000	2808.53	6010.04	-53.44	7.36	-20.99	11.85	1.13
503	0.00000	1195.44	1848.03	-73.63	7.84	-22.68	40.51	1.13
513	0.00038	4671.57	1387.98	-30.55	7.05	-18.98	na	na
523	bdl	bdl	3002.50	-79.00	7.94	-20.22	19.08	1.94

Table S2. Sedimentary TOC (in mg/g), $TOC/TN_{(molar)}$, $\delta^{13}C_{TOC}$ (‰) and $\delta^{15}N_{TN}$ (‰) in the studied sediment core (SSD070/7/GC6). bdl= below detection limit, na= not analyzed.

Depth (cmbsf)	Fe_D (mg/g)	Fe_{Asc} (mg/g)	TOC (mg/g)	TOC/TN (molar)	$\delta^{13}C_{TOC}$ (‰ VPDB)	Depth (cmbsf)	$\delta^{15}N_{TN}$ (‰VPDB)
0.5	4.54	3.11	26.05	11.31	-22.61	0.5	7.7
4.5	3.72	2.20	24.27	10.50	-22.64	28.5	7.2
8.5	1.55	0.93	24.71	11.55	-23.64	60.5	5.6
12.5	1.91	1.49	24.52	11.47	-23.01	123	6.4
16.5	1.69	1.37	23.69	10.77	-23.00	133	5.4
20.5	2.17	1.48	19.49	12.19	-21.24	143	6.5
24.5	1.58	1.57	22.38	11.74	-22.41	193	7.7
28.5	2.07	na	22.53	10.89	-22.48	203	5.5
32.5	3.78	2.91	22.56	11.62	-21.38	213	5.1
36.5	2.53	na	17.89	12.24	-22.63	248.5	7.0
40.5	3.57	2.82	21.87	12.36	-21.29	263	3.3
44.5	2.79	na	17.66	9.01	-22.60	273	7.0
48.5	4.21	1.47	20.62	12.64	-21.42	283	4.4
52.5	2.82	1.99	20.08	11.63	-22.45	296.5	7.2
56.5	2.52	na	23.74	11.19	-20.86	323	2.3
60.5	3.35	2.52	23.47	12.58	-21.96	333	7.2
64.5	2.51	na	20.27	12.63	-20.86	353	3.9
68.5	1.90	1.31	15.94	9.41	-20.83	373	0.2
72.5	2.50	na	21.50	12.12	-20.74	383	-0.3
76.5	3.33	1.11	19.42	10.49	-22.10	392.5	-3.6

80.5	2.82	na	19.77	12.27	-20.92	408.3	-0.1
84.5	3.69	3.17	19.84	12.70	-20.77	433	2.5
88.5	2.44	na	20.14	13.20	-20.69	443	0.3
92.5	2.79	1.72	18.58	12.32	-20.70	453	1.6
96.5	5.92	na	22.25	11.57	-21.87	472.5	-0.3
100.5	1.04	1.00	21.86	12.77	-20.95	492.5	0.6
104.5	3.24	na	20.92	12.76	-21.75	504.5	3.6
116.5	3.03	0.84	18.75	13.31	-21.54	523.5	1.0
120.5	5.56	na	11.71	8.20	-21.24		
124.5	1.92	1.07	13.78	9.78	-21.31		
133	1.53	0.28	25.41	10.50	-21.37		
136.5	1.40	0.77	19.78	na	-21.36		
140.5	3.15	0.78	23.45	14.04	-21.23		
144.5	1.16	na	21.30	14.55	-21.62		
148.5	2.80	1.52	10.66	13.13	-21.45		
153.5	2.11	na	13.06	13.97	-22.14		
156.5	2.03	0.68	20.90	15.43	-22.45		
160.5	1.07	na	24.01	13.11	-24.20		
164.5	3.30	0.70	27.16	na	-22.55		
168.5	3.52	1.56	25.45	16.37	-22.79		
172.5	1.77	1.03	19.59	17.02	-22.48		
176.5	1.34	0.57	18.33	16.27	-22.32		
180.5	1.86	0.72	29.60	19.39	-22.05		
184.5	4.32	1.07	20.67	15.03	-23.45		
188.5	3.96	1.61	25.35	21.41	-23.38		

192.5	2.53	na	16.34	12.30	-22.70		
196.5	2.90	1.14	18.01	22.01	-23.78		
200.5	1.54	0.59	22.68	19.98	-20.98		
203	2.50	0.27	19.48	16.05	-24.19		
208.5	2.17	na	17.36	13.77	-22.69		
212.5	2.37	1.10	17.54	16.92	-22.95		
216.5	2.12	1.23	14.61	12.90	-23.16		
220.5	2.12	0.92	25.43	16.98	-23.66		
223	1.92	0.53	21.89	16.94	-23.08		
228.5	1.40	0.59	22.58	17.37	-23.02		
232.5	3.04	na	22.28	na	-23.07		
236.5	2.65	1.10	23.28	na	-24.34		
240.5	2.45	0.01	16.51	15.12	-22.82		
244.5	4.18	0.77	18.54	14.77	-22.88		
248.5	2.42	na	14.17	12.53	na		
252.5	3.39	0.43	12.52	10.65	-22.73		
256.5	2.77	0.37	16.62	14.32	-22.71		
260.5	2.61	0.35	12.34	14.54	-23.01		
264.5	3.68	na	16.02	14.38	-23.16		
268.5	3.14	1.87	11.87	13.26	-23.96		
272.5	1.60	0.32	13.69	13.86	-24.65		
276.5	2.70	0.32	18.61	15.02	-22.56		
280.5	0.54	na	15.10	13.85	-22.87		
284.5	3.45	0.38	15.39	14.04	-23.29		
288.5	0.87	0.21	16.74	15.72	-22.83		

293	2.27	na	14.56	15.27	-22.67		
300.5	2.73	0.94	20.63	20.48	-23.58		
303	3.21	1.77	17.13	17.07	-23.66		
304.5	1.40	na	19.35	20.28	na		
308.5	4.30	0.54	16.12	17.23	-23.84		
312.5	3.97	na	15.77	15.83	-23.07		
316.5	5.77	na	12.70	bdl	-23.05		
323	2.83	na	14.62	14.99	-23.09		
324.5	3.59	1.91	10.91	14.62	na		
328.5	3.07	na	31.30	bdl	-22.95		
333	1.74	0.46	11.35	11.33	-23.36		
336.5	3.14	0.82	19.31	20.39	-22.91		
340.5	0.96	0.84	13.69	13.69	-22.82		
344.5	0.70	na	11.36	18.63	-22.90		
348.5	1.25	0.39	15.93	15.53	-22.93		
352.5	5.38	0.47	15.32	15.59	na		
356.5	3.13	0.57	15.04	16.97	-22.68		
360.5	2.54	na	4.65	4.95	-22.37		
364.5	4.86	0.71	16.06	bdl	-24.30		
368.5	3.66	na	7.97	14.91	-22.72		
373	2.05	0.33	na	na	-22.27		
376.5	4.83	na	12.97	bdl	-23.68		
380.5	5.84	1.68	9.79	14.64	-22.87		
383	4.40	0.47	9.68	14.51	-25.21		
388.5	4.02	1.30	4.86	6.80	-23.52		

393	5.12	0.52	12.22	20.87	-23.06		
396.5	4.02	2.24	4.77	bdl	-25.66		
400.5	1.74	na	3.16	7.10	-23.50		
404.5	2.00	0.83	1.45	3.47	-22.86		
408.5	2.02	na	8.03	16.81	-22.99		
412.5	4.51	1.16	9.85	bdl	-23.19		
416.5	3.56	1.99	9.12	12.23	-24.40		
420.5	1.79	0.92	9.35	13.36	-23.15		
424.5	3.13	1.33	13.04	15.54	-23.72		
428.5	4.67	3.33	12.79	18.07	na		
432.5	4.12	na	15.27	18.04	-25.10		
436.5	5.17	3.33	12.21	16.73	-23.77		
440.5	3.88	na	12.78	16.20	-24.94		
443	3.38	1.18	12.89	10.83	-25.93		
448.5	4.01	na	14.49	16.14	-25.43		
452.5	3.37	2.84	13.95	17.29	-24.97		
456.5	2.30	na	12.66	16.33	-25.06		
460.5	4.99	1.47	13.68	18.14	-23.95		
463	6.03	0.31	14.95	15.90	-24.86		
468.5	2.42	1.24	10.80	27.32	-23.90		
473	4.27	0.63	14.37	18.14	na		
476.5	2.01	0.68	15.48	20.26	-23.94		
479.5	3.97	na	12.36	14.69	-24.81		
484.5	1.41	0.40	17.54	19.03	-24.04		
488.5	0.82	na	13.88	18.28	-25.21		

492.5	4.34	0.45	14.90	16.97	-23.66		
496.5	1.20	na	9.58	11.79	-24.42		
500.5	3.47	2.87	14.95	16.31	-23.91		
503	4.15	0.51	14.61	14.66	-24.95		
510.5	6.48	4.27	9.72	14.38	-24.50		
514.5	6.68	na	12.48	12.97	-24.01		
517.5	7.18	1.30	13.62	16.71	na		
523	4.25	0.59	10.01	14.67	-24.41		
524.5	3.21	1.2	16.13	19.92	-24.46		

101

Table S3. Proportion of metagenomic reads from individual sediment samples of SSK42/9 matching sequences from *Candidatus* Methanoperedens genomes.

Sediment-depth from where metagenomes were sequenced (cmbsf)	BioSample accession number of the metagenome	Sample fraction of the metagenome	Run accession number for the sample fraction	*Candidatus* Methanoperedens genome GCA_003104905.1		*Candidatus* Methanoperedens genome GCA_001317315.1	
				Percentage of metagenomic reads mapping* onto the genome	Percentage of the genome covered by the mapped* metagenomic reads	Percentage of metagenomic reads mapping* onto the genome	Percentage of the genome covered by the mapped* metagenomic reads
0	SAMN04442233	1st replicate	SRR3872933	0.01	0.52	0.01	0.52
		2nd replicate	SRR3872934				
19	SAMN04442236	1st replicate	SRR3884351	0.02	0.59	0.02	0.59
		2nd replicate	SRR3884355				
50	SAMN04442238	1st replicate	SRR3884357	0.03	0.45	0.03	0.45
		2nd replicate	SRR3884359				
115	SAMN04442241	1st replicate	SRR3884468	0.03	0.24	0.03	0.24
		2nd replicate	SRR3884472				
125	SAMN04442242	1st replicate	SRR3884479	0.03	0.51	0.03	0.51
		2nd replicate	SRR3884488				
145	SAMN04442244	1st replicate	SRR3884538	0.03	0.43	0.03	0.43
		2nd replicate	SRR3884540				
155	SAMN04442245	1st replicate	SRR3884542	0.03	0.47	0.03	0.47
		2nd replicate	SRR3884544				
180	SAMN04442246	1st replicate	SRR3884546	0.03	0.40	0.03	0.40
		2nd replicate	SRR3884547				
225	SAMN04442248	1st replicate	SRR3884548	0.03	0.48	0.03	0.48
		2nd replicate	SRR3884552				
255	SAMN04442250	1st replicate	SRR3884553	0.03	0.61	0.03	0.61
		2nd replicate	SRR3884554				

* The duplicate metagenomic datasets available for each sediment sample were merged and reads were matched with sequences from the Methanoperedens genomes using the short-read alignment software Bowtie2 v2.2.5 (Langmead et al., 2012) with default parameter.

Two species-level entities affiliated to the uncultivated archaeon *Candidatus* Methanoperedens have been reported thus far for potential abilities to harness anaerobic methane oxidation to the reduction of Fe (III) (Ettwig et al., 2016; Cai et al., 2018). When the metagenomes sequenced along a ~3 m sediment core (SSK42/9) collected from the shallow seasonal hypoxic zone of the west coast of India (water depth: 31 m; GPS coordinates: 16°13.56' N and 73°19.16' E) were searched for signatures corresponding to sequences from the two *Candidatus* Methanoperedens genomes available in the GenBank (assembly numbers GCA_003104905.1 and GCA_001317315.1), 0.01% to 0.03% of reads from the individual metagenomic datasets of SSK42/9 mapped onto each of the genome with coverage breadth ranges from 0.24% to 0.61% (Table S3). The genome-metagenome correspondence data from SSK42/9 highlighted the presence of Methanoperedens-like archaea in the sulfidic coastal sediments of Eastern Arabian Sea (west coast of India).

References

References for Figure 1a in the main text

Aromokeye, D. A., Kulkarni, A. C., Elvert, M., Wegener, G., Henkel, S., Coffinet, S., Eickhorst, T., Oni, O. E., Richter-Heitmann, T., and Schnakenberg, A.: Rates and microbial players of iron-driven anaerobic oxidation of methane in methanic marine sediments, Frontiers in Microbiology, 10, 3041, https://doi.org/10.3389/fmicb.2019.03041, 2019.

Beal, E. J., House, C. H., and Orphan, V. J.: Manganese-and iron-dependent marine methane oxidation, Science, 325, 184-187, https://doi.org/10.1126/science.1169984, 2009.

Egger, M., Rasigraf, O., Sapart, C. J., Jilbert, T., Jetten, M. S. M., Rockmann, T., Van der Veen, C., Banda, N., Kartal, B., and Ettwig, K. F.: Iron-mediated anaerobic oxidation of methane in brackish coastal sediments, Environmental science & technology, 49, 277-283, https://doi.org/10.1021/es503663z, 2015a.

Egger, M., Jilbert, T., Behrends, T., Rivard, C., and Slomp, C. P.: Vivianite is a major sink for phosphorus in methanogenic coastal surface sediments, Geochimica et Cosmochimica Acta, 169, 217-235, https://doi.org/10.1016/j.gca.2015.09.012, 2015b.

Egger, M., Kraal, P., Jilbert, T., Sulu-Gambari, F., Sapart, C. J., Röckmann, T., and Slomp, C. P.: Anaerobic oxidation of methane alters sediment records of sulfur, iron and phosphorus in the Black Sea, Biogeosciences, https://doi.org/10.5194/bg-13-5333-2016, 2016a.

Egger, M., Lenstra, W., Jong, D., Meysman, F. J. R., Sapart, C. l. J., Van der Veen, C., Röckmann, T., Gonzalez, S., and Slomp, C. P.: Rapid sediment accumulation results in high methane effluxes from coastal sediments, PloS one, 11, e0161609, https://doi.org/10.1371/journal.pone.0161609, 2016b.

Egger, M., Hagens, M., Sapart, C. l. J., Dijkstra, N., van Helmond, N. A. G. M., MogollÃ³n, J. M., Risgaard-Petersen, N., van der Veen, C., Kasten, S., and Riedinger, N.: Iron oxide reduction in methane-rich deep Baltic Sea sediments, Geochimica et Cosmochimica Acta, 207, 256-276, https://doi.org/10.1016/j.gca.2017.03.019, 2017.

Li, J., Li, L., Bai, S., Ta, K., Xu, H., Chen, S., Pan, J., Li, M., Du, M., and Peng, X.: New insight into the biogeochemical cycling of methane, S and Fe above the Sulfate-Methane Transition Zone in methane hydrate-bearing sediments: A case study in the Dongsha area, South China Sea, Deep Sea Research Part I: Oceanographic Research Papers, 145, 97-108, https://doi.org/10.1016/j.dsr.2019.01.011, 2019.

Luo, M., Torres, M. E., Hong, W.-L., Pape, T., Fronzek, J., Kutterolf, S., Mountjoy, J. J., Orpin, A., Henkel, S., and Huhn, K.: Impact of iron release by volcanic ash alteration on carbon cycling in sediments of the northern Hikurangi margin, Earth and Planetary Science Letters, 541, 116288, https://doi.org/10.1016/j.epsl.2020.116288, 2020.

Oni, O., Miyatake, T., Kasten, S., Richter-Heitmann, T., Fischer, D., Wagenknecht, L., Kulkarni, A., Blumers, M., Shylin, S. I., and Ksenofontov, V.: Distinct microbial populations are tightly linked to the profile of dissolved iron in the methanic sediments of the Helgoland mud area, North Sea, Frontiers in Microbiology., 6, 365, https://doi.org/10.3389/fmicb. 2015.00365, 2015.

Orphan, V. J., Ussler Iii, W., Naehr, T. H., House, C. H., Hinrichs, K. U., and Paull, C. K.: Geological, geochemical, and microbiological heterogeneity of the seafloor around methane vents in the Eel River Basin, offshore California, Chemical Geology, 205, 265-289, https://doi.org/10.1016/j.chemgeo.2003.12.035, 2004.

Riedinger, N., Formolo, M. J., Lyons, T. W., Henkel, S., Beck, A., and Kasten, S.: An inorganic geochemical argument for coupled anaerobic oxidation of methane and iron reduction in marine sediments, Geobiology, https://doi.org/10.1111/gbi.12077, 2014.

Scheller, S., Yu, H., Chadwick, G. L., McGlynn, S. E., and Orphan, V. J.: Artificial electron acceptors decouple archaeal methane oxidation from sulfate reduction, Science, 351, 703-707, https://doi.org/10.1126/science.aad7154, 2016.

Slomp, C. P., Mort, H. P., Jilbert, T., Reed, D. C., Gustafsson, B. G., and Wolthers, M.: Coupled dynamics of iron and phosphorus in sediments of an oligotrophic coastal basin and the impact of anaerobic oxidation of methane, PloS one, 8, e62386, https://doi.org/10.1371/journal.pone.0062386, 2013.

Wankel, S. D., Adams, M. M., Johnston, D. T., Hansel, C. M., Joye, S. B., and Girguis, P. R.: Anaerobic methane oxidation in metalliferous hydrothermal sediments: influence on carbon flux and decoupling from sulfate reduction, Environmental microbiology, 14, 2726-2740, https://doi.org/10.1111/j.1462-2920.2012.02825.x, 2012.

Xiao, X., Luo, M., Zhang, C., Zhang, T., Yin, X., Wu, X., Zhao, J., Tao, J., Chen, Z., and Liang, Q.: Metal-driven anaerobic oxidation of methane as an important methane sink in methanic cold seep sediments, Microbiology Spectrum, 11, e05337-05322, https://doi.org/10.1128/spectrum.05337-22, 2023.

Other References

Cai, C., Leu, A. O., Xie, G.-J., Guo, J., Feng, Y., Zhao, J.-X., Tyson, G. W., Yuan, Z., and Hu, S.: A methanotrophic archaeon couples anaerobic oxidation of methane to Fe (III) reduction, The ISME Journal, 12, 1929-1939, https://doi.org/10.1038/s41396-018-0109-x, 2018.

Ettwig, K. F., Zhu, B., Speth, D., Keltjens, J. T., Jetten, M. S. M., and Kartal, B.: Archaea catalyze iron-dependent anaerobic oxidation of methane, Proceedings of the National Academy of Sciences of the United States of America, 113, 12792-12796, https://doi.org/10.1073/pnas.-1609534113, 2016.

Fernandes, S., Mazumdar, A., Peketi, A., Anand, S. S., Rengarajan, R., Jose, A., Manaskanya, A., Carvalho, M. A., and Shetty, D.: Sulfidization processes in seasonally hypoxic shelf sediments: a study off the West coast of India, Marine and Petroleum Geology, 117, 104353, https://doi.org/10.1016/j.marpetgeo.2020.104353, 2020.

Hensen, C., Zabel, M., Pfeifer, K., Schwenk, T., Kasten, S., Riedinger, N., Schulz, H., and Boetius, A.: Control of sulfate pore-water profiles by sedimentary events and the significance of anaerobic oxidation of methane for the burial of sulfur in marine sediments, Geochimica et Cosmochimica Acta, 67, 2631-2647, https://doi.org/10.1016/S0016-7037(03)00199-6, 2003.

Karisiddaiah, S., Veerayya, M., and Vora, K.: Seismic and sequence stratigraphy of the central western continental margin of India: late-Quaternary evolution, Marine Geology, 192, 335-353, https://doi.org/10.1016/S0025-3227(02)00591-1, 2002.

Kurian, S., Agnihotri, R., Borole, D. V., Naqvi, S., Ferreira, A. M., and Vale, C.: Possible solar control on primary production along the Indian west coast on decadal to centennial timescale, Journal of Quaternary Science, 24, 109-116, https://doi.org/10.1002/jqs.1193, 2009.

Langmead, B. and Salzberg, S. L.: Fast gapped-read alignment with Bowtie 2, Nature methods, 9, 357-359, https://doi.org/10.1038/nmeth.1923, 2012.

Mazumdar, A., Peketi, A., Joao, H., Dewangan, P., Borole, D. V., and Kocherla, M.: Sulfidization in a shallow coastal depositional setting: Diagenetic and palaeoclimatic implications, Chemical Geology, 322, 68-78, https://doi.org/10.1016/j.chemgeo.2012.06.005, 2012.

Nair, R. R., Hashimi, N. H., Kidwai, R. M., Guptha, M. V. S., Paropkari, A. L., Ambre, N. V., Muralinath, A. S., Mascarenhas, A., and D'Costa, G. P.: Topography and sediments of the western continental shelf of India-Vengurla to Mangalore, 1978.

Naqvi, S., Jayakumar, D., Narvekar, P., Naik, H., Sarma, V., D'Souza, W., Joseph, S., and George, M.: Increased marine production of N2O due to intensifying anoxia on the Indian continental shelf, Nature, 408, 346-349, https://doi.org/10.1038/35042551, 2000.

Naqvi, S. W. A., Naik, H., Jayakumar, D., Shailaja, M., and Narvekar, P.: Seasonal oxygen deficiency over the western continental shelf of India, Past and present water column anoxia, 195-224, https://doi.org/10.1007/1-4020-4297-3_08, 2006.

Nigam, R., Khare, N., and Nair, R.: Foraminiferal evidences for 77-year cycles of droughts in India and its possible modulation by the gleissberg solar cycle, Journal of Coastal Research, 11, 1099-1107, https://www.jstor.org/stable/4298414, 1995.

Rao, V. P. and Nair, R. R.: Microbial origin of the phosphorites of the western continental shelf of India, Marine Geology, 84, 105-110, https://doi.org/10.1016/0025-3227(88)90128-4, 1988.

Rao, V. P. and Wagle, B.: Geomorphology and surficial geology of the western continental shelf and slope of India: A review, Current Science, 73, 330-350p, https://www.jstor.org/stable/24100364, 1997.

Sebastian, T., Nath, B. N., Naik, S., Borole, D. V., Pierre, S., and Yazing, A. K.: Offshore sediments record the history of onshore iron ore mining in Goa State, India, Marine Pollution Bulletin, 114, 805-815, https://doi.org/10.1016/j.marpolbul.2016.10.075, 2017.

Siddiquie, H., Rao, D. G., Vora, K., and Topgi, R.: Acoustic masking in sediments due to gases on the western continental shelf of India, Marine Geology, 39, M27-M37, https://doi.org/10.1016/0025-3227(81)90023-2, 1981.

Wagle, B., Vora, K., Karisiddaiah, S., Veerayya, M., and Almeida, F.: Holocene submarine terraces on the western continental shelf of India; Implications for sea-level changes, Marine Geology, 117, 207-225, https://doi.org/10.1016/0025-3227(94)90016-7, 1994.